JOURNAL OF GUIDANCE, CONTROL, AND DYNAMICS
Vol. 21, No. 5, September–October 1998

Effective Selection of Piezoceramic Actuators for an Experimental Flexible Wing

K. B. Lim,* R. C. Lake,† and J. Heeg‡
NASA Langley Research Center, Hampton, Virginia 23681

The effectiveness of individual or subsets of piezoceramic actuators are investigated in terms of their contributions to the joint controllability and observability for a fixed set of sensors. The method used is based on the decomposition of the Hankel singular values in terms of individual sensor and actuator combinations for flexible structures. The degree of participation of the individual structural modes in the flutter control problem is used to weigh the actuator selection metric in the feedback loop. Simulation results based on H_2 and H_∞ control law designs indicate that closed loop performance can be improved significantly and the performance improvement is independent of the particular type of control law.

I. Introduction

THE piezoceramic aeroelastic response tailoring investigation (PARTI) wind-tunnel model at NASA Langley Research Center[1,2] is an aeroelastic testbed for active control of flutter via piezoceramic actuators. Unlike traditional approaches to active flutter control using control surfaces that are usually predetermined in their size and location on the wing, the recent technology of bonding potentially many discrete piezoceramic actuators directly on a three-dimensional wing structure motivates the question of effective locations in terms of controllabilty and observability. Physically, this effectiveness translates to requiring less control effort and improved signal to noise ratio.

There are many issues affecting actuator selection for aeroelastic systems that go beyond the scope of this paper. For instance, it is desirable to select actuators for designing control laws that can maintain stability and achieve desired performance over a wide range of operating conditions (Mach and dynamic pressure), which have potentially large differences in relative controllability and observability. A typical example is control reversal, where the controllability goes from positive to zero to negative over a range of speeds. Another issue affecting actuator selection is robustness and fault tolerance. The issue addressed in this paper is the selection of actuators at a single operating point. In particular, the number and location of piezoceramic actuators are addressed. The final goal is to identify effective actuator locations so that feedback control laws can be designed and implemented for improving the performance of an actively controlled flexible wing during predicted open-loop flutter. Knowing effective actuator locations will clearly necessitate a fewer number of actuators. Obviously, an exact minimal number of actuators must depend on a given desirable performance level for a particular control objective and constraints. For this reason, the goal of the actuator selection methodology considered in this paper is not to determine the minimal number, but rather to determine the relative effectiveness of individual or a set of actuators.

Many studies on actuator selection exist in the open literature and a partial list of citations can be found in Ref. 3. Among various actuator selection metrics that exist in the literature, an approach based on the joint controllability and observability that is quantified by Hankel singular values (HSV) is considered.[4] A detailed discussion of the physical interpretation and significance of HSV and grammian matrices is found in Ref. 3. Recently in Ref. 5, the use of a HSV formula as an actuator selection metric[6] was extended to flexible structures modeled in discrete time.[7]

In this investigation, the design and analysis algorithm for actuator selection, as formulated in Ref. 5, is examined from a flutter control design viewpoint. The outline of the paper is as follows. In Sec. II, the dynamical model for the PARTI wing used in the actuator selection is given. A nonparameterized identified model, from a wind-tunnel system identification experiment, is used to generate a reduced-order model that captures the modes involved in the wing flutter. Section III outlines the treatment of the active flutter control problem in the framework of a disturbance rejection problem. The HSV associated with each structural mode in the disturbance rejection problem is used to weigh the actuator selection metric. In Sec. IV, the metric used in the actuator selection is described. The metric is a weighted sum of HSV and is based on an approximate analytical formula. In Sec. V, two case studies for the PARTI wing model are outlined. For comparison purposes, optimal actuator selection is considered under different flutter control problem definitions. In Sec. VI, the analysis results in Sec. V are evaluated by applying two popular control strategies, namely, H_2 and H_∞, to design control laws to compare closed-loop performance. The dependence of the actuator selection results on the type of control law and control problem is examined. Section VII gives a few conclusions.

II. Flexible Wing Model

Figure 1 shows the sensors and actuators distributed on the PARTI wing model. This model has a total of 72 actuators adhered to both sides of the wing, which are hard-wired to actuate in 15 different groupings such that each group primarily affects one of the first three natural modes of the wing. The actuators are configured to impart differential bending moments to the wing and are able to affect both the bending and torsion modes of the model by virtue of the bend–twist elastic coupling inherent in the layup of the graphite epoxy wing spar, as well as the sweep angle of the wing design.

A model for the PARTI wing was identified from test data using an observer Markov-based technique (OKID)[8] and was realized in state space using the eigensystem realization algorithm (ERA).[9] The identified model was obtained at a dynamic pressure of $q = 75$ psf with the model configured in the normal testing mode, where the flutter stopper was in the undeployed condition.[1,2] The sampling rate used was 200 Hz. Figure 2a shows the eigenvalues of the full model with 40 states. Without discriminating flutter modes from nonflutter modes, applying internal balancing to the 40 state model using all inputs (w, u) to all outputs (z, y) indicated that no state

Presented as Paper 96-3758 at the AIAA Guidance, Navigation, and Control Conference, San Diego, CA, July 29–31, 1996; received May 5, 1997; revision received March 9, 1998; accepted for publication March 10, 1998.

*Research Engineer, Guidance and Control Branch, Flight Dynamics and Control Division. E-mail: k.b.lim@larc.nasa.gov.

†Research Engineer, Aeroelasticity Branch, Structures Division. E-mail: r.c.lake@larc.nasa.gov.

‡Research Engineer, Aeroelasticity Branch, Structures Division. E-mail: j.heeg@larc.nasa.gov.

Table 1 Eigenvalues of reduced PARTI model at q = 75 psf and 200 Hz

Mode no.	Frequency (in Nyquist)	Eigenvalues
1	0.0503	$0.9762 \pm 0.1555i$
2	0.0955	$0.9297 \pm 0.2876i$
3	0.1757	$0.8291 \pm 0.5105i$
4	0.3558	$0.4243 \pm 0.8720i$

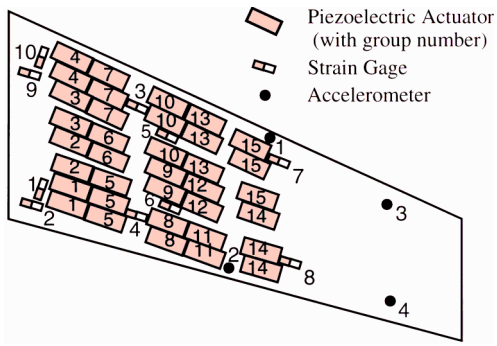

Fig. 1 Location of strain gauges and piezoceramic actuators on PARTI model.

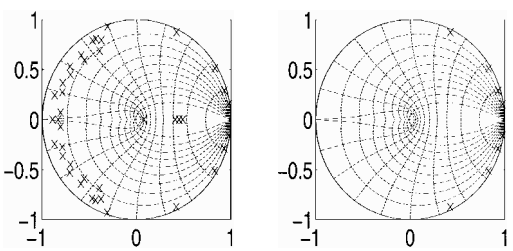

Fig. 2 Eigenvalues of PARTI model at q = 75 psf and 200 Hz sampling rate.

can be reduced without incurring a significant error in terms of its singular values.[10] Most of the modes appear to be lightly damped high-frequency (greater than half of Nyquist frequency of 100 Hz) modes with several well-damped states on the real axis. Figure 2b shows the poles of the reduced-order model after truncating well-damped states that lie on the real axis and all higher frequency modes that are beyond 50 Hz (half of Nyquist frequency). The rationale for the truncation is that the important aeroelastic modes are well below 50 Hz and the overdamped real poles contribute very little to the overall response. The reduced model finally used in the actuator selection study consisted of four modes. Table 1 shows the values of the discrete eigenvalues of the reduced eight-state model used in the actuator selection study. Modes 1 and 3 correspond to the first two bending modes, whereas mode 2 corresponds to the first torsional mode. The first torsional and bending modes eventually coalesce, leading to flutter.

III. Flutter Control and Disturbance Rejection

Flutter is an undesirable oscillatory response associated with a dynamic instability due to coupling between the wing structural deformation and the aerodynamic loading. Under a given condition, for example, at a dynamic pressure near the onset of flutter, the response, stability margins, controllability, and observability can be predicted by a linearized model. In this study, a linear model of the PARTI wing at a condition near flutter ($q = 75$ psf) is used. Flutter occurs at $q = 76$ psf and is manifested as a coalescence of the first bending and first torsion natural modes of the PARTI wing model.

Active control of flutter is viewed as a disturbance rejection problem for a linearly unstable or nearly unstable system from the controls perspective.

Figure 3 shows a schematic of the disturbance rejection problem, where

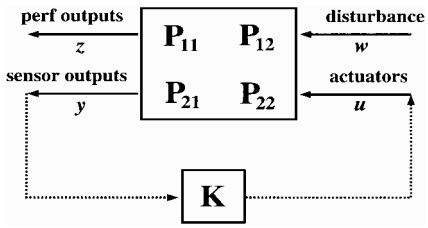

Fig. 3 Flutter control as a disturbance rejection problem.

$$\begin{Bmatrix} z \\ y \end{Bmatrix} = \begin{bmatrix} P_{11} & P_{12} \\ P_{21} & P_{22} \end{bmatrix} \begin{Bmatrix} w \\ u \end{Bmatrix} = P \begin{Bmatrix} w \\ u \end{Bmatrix} \tag{1}$$

As a necessary starting point for the actuator selection problem addressed, the disturbance source w, the output response defining the performance z, and a set of sensor outputs used for feedback y are assumed known. For this investigation, disturbance inputs w are chosen as the piezoceramic actuators numbers 7 and 8, whereas two different sets of outputs are used as the performance variables z that define the flutter response (strain gauges 1 and 2 for case 1 and strain gauges 9 and 10 for case 2). Strain gauges 1 and 2 are the measured sensor outputs y used for output feedback control. The task is to determine the most effective set of actuators u among the given set of piezoceramic actuators. For this study, only the first eight actuators were considered for simplicity.

Note that, in a general multivariable control design framework,[11] the augmented plant P is assumed given, and the problem is to design a suitable controller K to minimize a suitable norm of the transfer function matrix from the disturbance to the performance outputs. The difficulty in the actuator selection problem is that only P_{11} and P_{21} are known from the disturbance rejection definition and the fixed set of sensors assumed. The remaining models, P_{12} and P_{22}, i.e., the effect of actuators to performance and sensor outputs, will be defined by a judicious selection of actuators.

Suppose all candidate actuator locations are given and a determination of the most effective actuator configuration for a fixed number of actuators is desired. A direct approach to selecting efficient actuators to optimize a given closed-loop performance metric will involve computing an optimal control law for each candidate configuration of actuators and then selecting the configuration with the optimal–optimal configuration. However, the computational effort necessary to solve the combinatory problem with optimal controller design may not be trivial. To illustrate, consider the computational requirements for placing exactly 8 actuators on 48 candidate locations, based on optimal linear quadratic Gaussian (LQG) metric. Computing all combinations requires solving $C(48, 8) = 377, 348, 994$ LQG control problems. Therefore, if it takes 10^{-2} s to solve an LQG problem, the total time needed will be roughly 43 days. Obviously, if an optimal H_∞ controller is to be used, the computational effort necessary would be a bit more challenging. The computational effort necessary in a combinatory type search for a global optimum may be inconvenient, even for a modest size problem, because the computational effort grows factorially with the size of the problem.[12] Furthermore, a different number of actuators, for example, 6 instead of 8, will likely require a completely new set of calculations. A partial list of earlier attempts using the closed-loop approach can be found in Ref. 3.

The alternative approach, which is followed in this study, is to select actuators from their open-loop characteristics. This open-loop-based approach does not require the simultaneous consideration of a control law because closed-loop performance is not directly considered. Instead, the open-loop approach will suggest effective actuator and sensor configurations based on the degree of joint controllability and observability for the open-loop system and, therefore, should apply for any type of control law.

IV. Actuator Placement Metric/Strategy

A. HSV of Flexible Structures

For a general linear time invariant multivariable system, the HSV and the corresponding principal directions depend on the sets of inputs and outputs given. This means that, in general, there is no

relation between any HSV from a given set of inputs and outputs to a different set. However, for flexible structures, the principal directions correspond individually to modal states[3,5–7] and are almost independent of the inputs and outputs. The innovation of the selection metric considered in this paper is that the HSV from the inputs and outputs characterizing flutter response are used to weigh the summed HSV from candidate actuators to sensor sets. This section will briefly overview the results given in detail in Ref. 5, beginning with a definition of a state-space model that HSV is based on.

Let the quadruple (A_z, B_z, C_z, D_z) be the reduced discrete state-space model. The pair (z_i, v_i) are the ith eigenvalue and eigenvector of A_z and T is the sampling period. For a lightly damped flexible structure, the ith discrete eigenvalue lies just inside the unit circle and is written as

$$z_i = \exp(-\delta_i + j\psi_i)T \tag{2}$$

where $-\delta_i + j\psi_i$ corresponds to the ith pole of an equivalent continuous system. By using the similarity transformation matrix

$$V = [r_1, \ldots, r_n] \tag{3}$$

where $r_i = [\mathrm{Re}(v_i) - \mathrm{Im}(v_i)]$, the state equations are block diagonalized to the form

$$x(k+1) = \tilde{A}x(k) + \tilde{B}u(k) \tag{4}$$

$$y(k) = \tilde{C}x(k) + \tilde{D}u(k) \tag{5}$$

where

$$\tilde{A} = \text{blk-diag}(\tilde{A}_1(T), \ldots, \tilde{A}_n(T)) \tag{6}$$

$$\tilde{B} = V^{-1}B_z, \qquad \tilde{C} = C_z V, \qquad \tilde{D} = D_z \tag{7}$$

and

$$\tilde{A}_i = \begin{bmatrix} \mathrm{Re}(z_i) & -\mathrm{Im}(z_i) \\ \mathrm{Im}(z_i) & \mathrm{Re}(z_i) \end{bmatrix} \tag{8}$$

Note that the preceding similarity transformation does not give a balanced state but produces states whose eigenvectors (modes) approximately correspond to principal directions.[7]

For p actuators and q sensors, the input and output matrices consist of p columns and q rows, respectively,

$$B_z = \left[B_{z_1}, \ldots, B_{z_p}\right], \qquad C_z^T = \left[C_{z_1}^T, \ldots, C_{z_q}^T\right] \tag{9}$$

Partition the inverse state transformation matrix in Eq. (3) as follows:

$$V^{-T} = \left[l_1^T, \ldots, l_n^T\right] \tag{10}$$

where l_i are $2 \times 2n$ matrices made up of components of ith left eigenvector. For a stable and minimal system $(\tilde{A}, \tilde{B}, \tilde{C})$, the triple is balanced if its controllability and observability grammians are equal and diagonal[4]

$$W_{c_\infty} = W_{o_\infty} = \Gamma^2 \tag{11}$$

where $\Gamma^2 > 0$ is the diagonal matrix of the HSV of the system. The steady-state discrete time controllability grammian W_{c_∞} and observability grammian W_{o_∞} satisfy the following Sylvester equations:

$$\tilde{A}W_{c_\infty}\tilde{A}^T + \tilde{B}\tilde{B}^T = W_{c_\infty} \tag{12}$$

$$\tilde{A}^T W_{o_\infty}\tilde{A} + \tilde{C}^T\tilde{C} = W_{o_\infty} \tag{13}$$

Because of the diagonal dominance property of the discrete controllability and observability grammian for flexible structures, the square of the ith HSV can be approximated by[7]

$$\gamma_i^4 \cong \frac{\mathrm{tr}[\tilde{B}\tilde{B}^T]_{ii}\,\mathrm{tr}[\tilde{C}^T\tilde{C}]_{ii}}{(4\delta_i T)^2} \tag{14}$$

where $\delta_i = -(1/T)\mathrm{Re}(\ln z_i)$ is a measure of damping of ith mode and z_i is the ith eigenvalue of $\tilde{A}$. The subscripts ii are the ith 2×2 block of the $2n \times 2n$ matrices formed from the input and output matrices. It is shown in Ref. 7 that the simple approximate formula, Eq. (14), is quite accurate up to frequencies near 90% of the Nyquist frequency. Furthermore, the approximation arises due to assumptions of small damping and distinct frequencies.

B. Actuator Placement Metric

With reference to Fig. 3, let Γ_{wz}^2 be the HSV from the disturbance to the performance outputs

$$\Gamma_{wz}^2 = \mathrm{diag}\left(\gamma_{wz_1}^2, \ldots, \gamma_{wz_n}^2\right) \tag{15}$$

Note that Γ_{wz}^2 is completely determined by joint controllability and observability of the states in the system P_{11} due to the disturbance rejection input and output variables. These HSVs capture the relative degree of participation of each mode (or state) in the control problem performance. Hence, modes that are important in the disturbance rejection performance will correspond to larger singular values in Γ_{wz}^2. Furthermore, let Γ_{uy}^2 be the HSV for the feedback path, i.e., from p actuators to q sensors:

$$\Gamma_{uy}^2 = \mathrm{diag}\left(\gamma_{uy_1}^2, \ldots, \gamma_{uy_n}^2\right) \tag{16}$$

The HSVs Γ_{wz}^2 are completely determined by the joint controllability and observability of the states in the system P_{22} due to control inputs and feedback outputs. Hence, modes that participate strongly in the feedback loop will correspond to larger singular values in Γ_{uy}^2. Finally, define a third set of HSVs from a baseline reference set of feedback actuators to a baseline reference set of feedback sensors:

$$\bar{\Gamma}_{uy}^2 = \mathrm{diag}\left(\bar{\gamma}_{uy_1}^2, \ldots, \bar{\gamma}_{uy_n}^2\right) \tag{17}$$

From the preceding definition of the three sets of HSV, an actuator selection metric is constructed as the weighted sum

$$J \triangleq \sum_{i=1}^{n} \frac{\gamma_{uy_i}^4}{\bar{\gamma}_{uy_i}^4}\gamma_{wz_i}^4 \cong \sum_{k=1}^{p} J_k^{\mathrm{act}} \tag{18}$$

As noted earlier, because the principal directions of the HSV for a flexible structure are almost independent of the inputs and outputs, each HSV in all three sets corresponds to individual structural modes. Hence, the normalization by $\bar{\gamma}_{uy_i}^4$ and multiplication by γ_{uy}^4 to $\gamma_{wz_i}^4$ for each mode in Eq. (18) makes physical sense. Indeed, the analytical formula in Eq. (14), albeit an approximation, makes the association of each HSV to each structural mode clear. Of course, this is not so if the HSVs were calculated exactly by internal balancing transformation.

In Eq. (14), the contribution from the kth actuator is

$$J_k^{\mathrm{act}} = \sum_{i=1}^{n} f_{ik}^2 w_i^2 \tag{19}$$

where

$$f_{ik}^2 = \left\| l_i B_{z_k} \right\|_2^2 \tag{20}$$

and the weighting factor for the ith mode is

$$w_i^2 = \frac{1}{(4\delta_i T)^2}\frac{\gamma_{wz_i}^4}{\bar{\gamma}_{uy_i}^4}\sum_{j=1}^{q} g_{ij}^2 \tag{21}$$

where

$$g_{ij}^2 = \left\| C_{z_j} r_i \right\|_2^2 \tag{22}$$

Note that f_{ik} (g_{ij}) denotes the influence of the kth actuator (jth sensor) on the ith mode. Additional factors that contribute to the weighting factor include damping, significance with respect to disturbance rejection, and the reference HSV for the ith mode.

Note also that it is necessary to introduce these weights because the basic idea is to improve the joint controllability and observability for a set of modes, and not all modes are equally important physically. HSV can also vary by orders of magnitude and, therefore, a few physically irrelevent modes could dominate an unweighted scalar metric. Hence, the normalizing weight $\bar{\gamma}_{uy_i}^4$ is introduced to

make each HSV equally important, assuming no a priori physical knowledge of individual modes.

C. Selection Strategy

The goal is to maximize the weighted HSV metric J in Eq. (18) using a smaller subset of actuators. This amounts to the following combinatory problem: Given a candidate set of p actuator locations, find a subset of p_s actuators that maximizes J, specifically,

$$\max_{p_s} J \triangleq \sum_{i=1}^{n} \frac{\gamma_{uy_i}^4}{\bar{\gamma}_{uy_i}^4} \gamma_{wz_i}^4 \tag{23}$$

Because this metric can be approximately expressed as a sum of contributions from each actuator, the problem is essentially solved, albeit approximately. Hence, the most effective (in terms of J) subset of p_s ($\leq p$) actuators can be solved by inspecting a bar chart of J_k^{act}, $k = 1, \ldots, p$. An alternative strategy is to start with all p actuators and remove all ineffective actuators characterized by small numerical values of J_k^{act}.

Note that the metric/strategy do not require the a priori specification of the number of actuators and their locations. Instead, all candidate actuator locations are considered without a need to address all allowable combinations. This useful characteristic is in stark contrast to methods where the number of actuators needed must be fixed a priori before any analysis or optimization to determine their effective locations.

V. Results of Case Study

In this section, the results of applying the actuator selection method to the PARTI wing is given. Table 2 summarizes the input and output configurations defined for two cases considered. In both cases, the simulated external disturbance inputs are chosen as actuators 7 and 8, the feedback sensors are chosen as strains 1 and 2, and the same set of eight piezoceramic actuators are chosen to represent the set of all actuator candidates. As a choice of baseline reference HSV, all eight actuators and strains 1 and 2 were used in both cases. The two cases only differ by the definition of performance output variables, namely, strains 1 and 2 for case 1, whereas case 2 uses strains 9 and 10.

Figure 4 shows the disturbance rejection (left bar) and baseline HSV (right bar) for case 1. This baseline reference corresponds to the maximum attainable HSV using all eight actuators. For case 1, note the following:

Table 2 Input and output variables for actuator selection and control design

Variable	Case 1	Case 2
Perf output, z	Strains 1, 2	Strains 9, 10
Disturb input, w	Piezo 7, 8	Piezo 7, 8
Sensors, y	Strains 1, 2	Strains 1, 2
Actuators, u	Piezo 1:8	Piezo 1:8

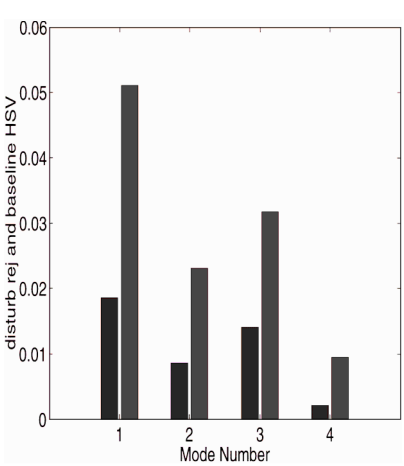

Fig. 4 HSVs for case 1, Γ_{wz} (left), $\bar{\Gamma}_{uy}$ (right).

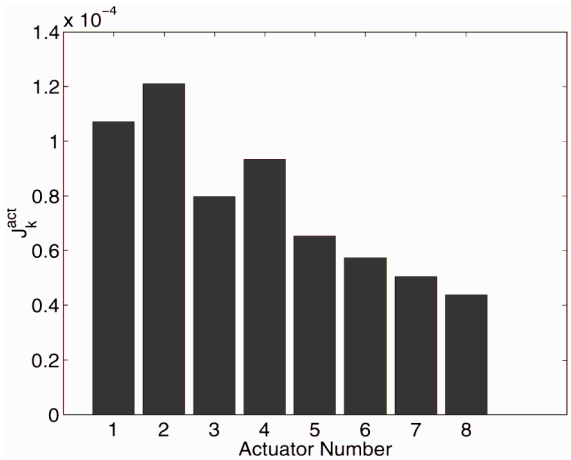

Fig. 5 Contribution of each actuator to overall performance for case 1, J_k^{act}.

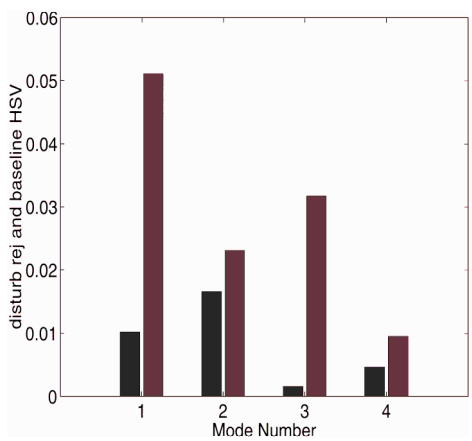

Fig. 6 HSVs for case 2, Γ_{wz} (left), $\bar{\Gamma}_{uy}$ (right).

1) All disturbance rejection and baseline HSVs show that all four modes are significantly controllable and observable.

2) The two most significant modes participating in the disturbance rejection path are modes 1 and 3 (first and second bending modes, respectively).

3) The relative sizes of the baseline HSV (all candidate actuators) indicates the sufficiency of the candidate set.

4) The baseline HSV is proportional to the disturbance rejection HSV. This is partly the result of the equivalence of the performance and sensor outputs.

Figure 5 shows the contributions from each actuator to the overall performance for case 1. The ranking of the individual actuators from the most to the least effective is as follows: 2, 1, 4, 3, 5, 6, 7, 8. The most effective (actuator 2) and the least effective (actuator 8) differ by less than an order of magnitude.

Figure 6 shows both the baseline (left bar) and disturbance rejection (right bar) HSV for case 2. For case 2, note the following:

1) All disturbance rejection and baseline HSVs show that all four modes are significantly controllable and observable.

2) The two most significant modes participating in the disturbance rejection path are modes 1 and 2 (first bending and first torsional modes, respectively).

3) The relative sizes of the baseline HSV (all candidate actuators) indicate the sufficiency of the candidate set.

4) Unlike case 1, the baseline HSV is not proportional to the disturbance rejection HSV.

Figure 7 shows the contributions from each actuator to the overall performance for case 2. The ranking of the individual actuators from the most to the least effective is as follows: 4, 3, 2, 5, 7, 6, 1, 8. The difference between the most effective (actuator 4) and the least effective (actuator 8) is more than an order of magnitude.

The designer is free to choose whatever number of effective actuators is needed from the contributions from each actuator. To evaluate

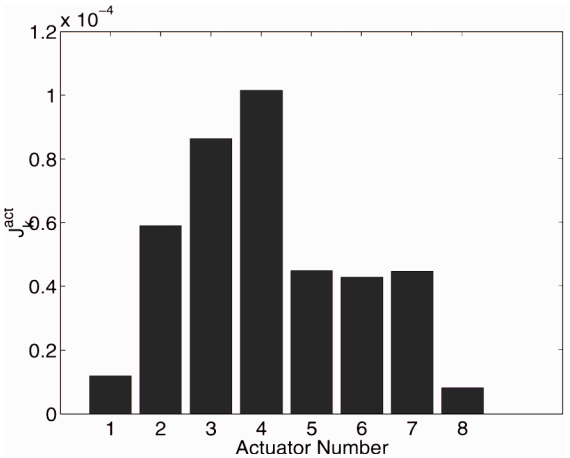

Fig. 7 Contribution of each actuator to overall performance for case 2, J_k^{act}.

the result of the effectiveness analysis, consider the two most effective actuators: actuators 1 and 2 for case 1 and actuators 3 and 4 for case 2. Note that the two optimal actuator locations do not correspond to the two disturbance inputs, which are actuators 7 and 8. Obviously, the two optimal actuator set locations are more effective than the two disturbance inputs in exciting/controlling the four modes of interest disturbed by actuators 7 and 8. The results of the selection are validated by designing various control laws and comparing their closed-loop performance in the next section.

VI. Controller Performance

A. Controller Design

Two types of control laws are used to evaluate the benefits of the preceding actuator selection results. For both cases, closed-loop performance is defined in terms of H_2 and H_∞ norms of the transfer function matrices from all external disturbances (process noise and measurement noise) to the regulated outputs (performance outputs and control effort). Figure 8 shows the block diagram used in the design of control laws based on optimal H_2 and H_∞ control theories.[13] Both control laws are designed based on the predicted best pair of actuators and the worst pair of actuators. The best pair of actuators for case 1 was (u_1, u_2), whereas the worst pair was (u_7, u_8). For case 2, the best pair of actuators was (u_3, u_4), whereas the worst pair was (u_1, u_8). By comparing the controlled performance between the predicted best and worst pairs for different control design strategies and output variables defining the performance, the proposed actuator selection metric and methodology can be evaluated. In all cases, the following weighting functions specified in the z domain are used:

$$W_w = 1.367 \times \frac{1 + z^{-1}}{1 - 0.7265 z^{-1}} I_{2\times 2} \tag{24}$$

$$W_m = 10^{-5} \times I_{2\times 2} \tag{25}$$

$$W_z = W_w \tag{26}$$

$$W_u = 0.1 \times I_{2\times 2} \tag{27}$$

The weights W_w and W_z are first-order digital Butterworth filters with cutoff frequency at 10 Hz, which corresponds to 0.1 of Nyquist frequency. The filter has a real pole at 0.7265 and a zero at -1, which defines the low-pass character. The cutoff frequency was selected to emphasize the disturbance rejection of the primary flutter modes (first two modes in Table 1). In this study for simplicity sake, possible influence from small measurement noise was in effect eliminated by choosing a small weight for noise, W_m. However, the weight matrix for control input W_u was chosen to be a constant to indicate that a significant control penalty was enforced over all frequencies and to avoid singular control.

B. Performance Comparison

Tables 3 and 4 show the closed-loop performance for both types of control laws and two types of performance outputs in cases 1 and 2,

Table 3 H_2 and H_∞ performance for case 1

	Case 1	
Controller	Best pair (u_1, u_2)	Worst pair (u_7, u_8)
H_2	3.32 (5.19)	3.81 (5.19)
H_∞	0.65 (2.82)	0.85 (2.82)

Table 4 H_2 and H_∞ performance for case 2

	Case 2	
Controller	Best pair (u_3, u_4)	Worst pair (u_1, u_8)
H_2	4.15 (5.49)	4.91 (5.49)
H_∞	0.63 (1.94)	1.29 (1.94)

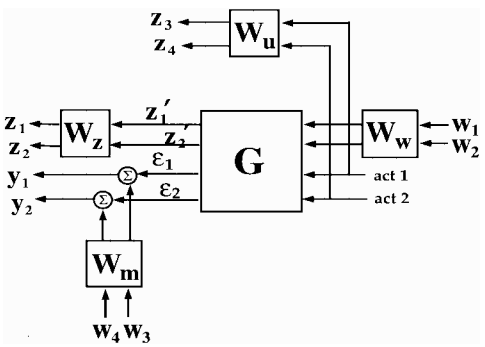

Fig. 8 Block diagram for control design.

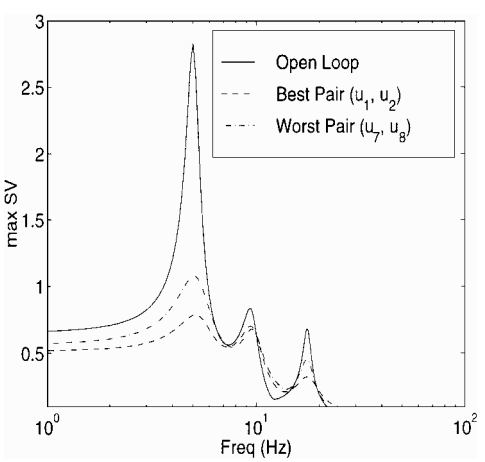

Fig. 9 Maximum singular value frequency response for case 1, H_2 control.

respectively. The H_2 controller minimizes the H_2 norm, which is the root mean square strain response, whereas the H_∞ controller minimizes the H_∞ norm, which is the worst-case strain response from a band-limited random external disturbance. The corresponding open-loop norms are shown in parentheses. It can be seen that in all four comparisons, the best pair consistently gives better closed-loop performance.

Figures 9 and 10 show the maximum singular values of the frequency-response matrix from all disturbances to all outputs for case 1. In both types of control law, the closed-loop performance metric using the best pair is significantly better than the performance metric corresponding to the worst pair of actuators. After changing the disturbance rejection definition as in case 2, as shown in Figs. 11 and 12, the best pair still produced significantly better closed-loop performance than the worst pair. Note that the responses for case 2 are clearly distinct from case 1 due to the difference in the performance output variables.

The preceding results indicate that the particular inputs and outputs used to characterize wing flutter strongly affect the actuator selection. This dependence is expected because the HSV of the

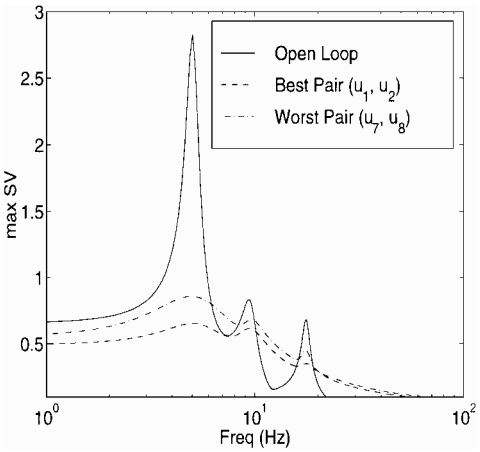

Fig. 10 Maximum singular value frequency response, for case 1, H_∞ control.

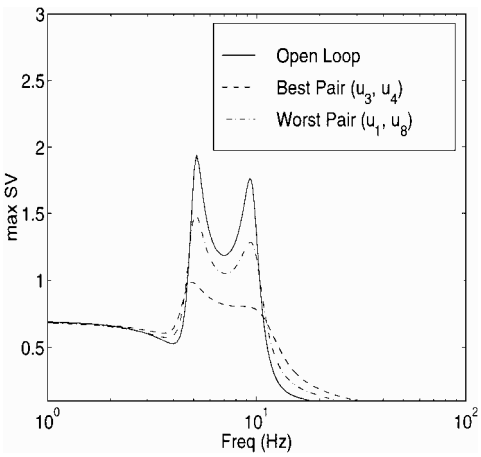

Fig. 11 Maximum singular value frequency response for case 2, H_2 control.

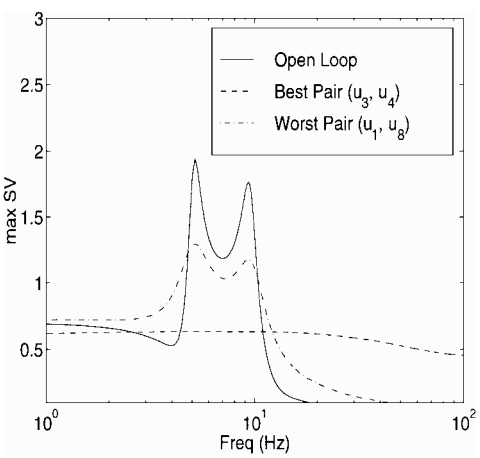

Fig. 12 Maximum singular value frequency response for case 2, H_∞ control.

disturbance rejection problem is used to weigh the HSV for the actuator selection. However, once the disturbance rejection problem is defined, the optimal actuator set gives improved closed-loop performance independent of the H_2 or H_∞ control law selected. This consistent improvement is partly the result of judiciously improved controllability and observability in the open-loop system.

VII. Conclusions

The actuator placement metric consisting of a weighted HSV in a disturbance rejection problem framework is intuitively attractive. The dramatic simplification of the placement metric for the flexible wing considered in this study, essentially trivially solves the necessary combinatory problem, albeit approximately. The simplicity and the intuitive characteristic of this approach should be contagious. For the experimental flexible wing considered, the simulation results convincingly demonstrated the benefit of the piezoceramic actuator selection methodology.

Acknowledgment

The authors would like to thank Martin Waszak of NASA Langley Research Center for a detailed review of this work and providing many valuable comments.

References

[1]Heeg, J., "Analytical and Experimental Investigation of Flutter Supression by Piezoelectric Actuation," NASA TP-3241, March 1993.

[2]Reich, G. W., and Crawley, E. F., "Design and Modeling of an Active Aeroelastic Wing," Space Engineering Research Center, Rept. 4-94, Massachusetts Inst. of Technology, Cambridge, MA, Feb. 1994.

[3]Lim, K. B., and Gawronski, W., "Actuator and Sensor Selection for Control of Flexible Structures," *Control and Dynamics Systems*, edited by C. T. Leondes, Vol. 57, Academic, San Diego, CA, 1993, pp. 109–152.

[4]Moore, B. C., "Principal Component Analysis in Linear Systems: Controllability, Observability and Model Reduction," *IEEE Transactions on Automatic Control*, Vol. 26, No. 1, 1981, pp. 17–32.

[5]Lim, K. B., "Disturbance Rejection Approach to Actuator and Sensor Placement," *Journal of Guidance, Control, and Dynamics*, Vol. 20, No. 1, 1997, pp. 202–204.

[6]Gawronski, W., and Lim, K. B., "Balanced Actuator and Sensor Placement for Flexible Structures," *International Journal of Control*, Vol. 65, No. 1, 1996, pp. 131–145.

[7]Lim, K. B., and Gawronski, W., "Hankel Singular Values of Flexible Structures in Discrete Time," *Journal of Guidance, Control, and Dynamics*, Vol. 19, No. 6, 1996, pp. 1370–1377.

[8]Juang, J.-N., Phan, M., Horta, L. G., and Longman, R. W., "Identification of Obser/Kalman Filter Markov Parameters: Theory and Experiments," *Journal of Guidance, Control, and Dynamics*, Vol. 16, No. 2, 1993, pp. 320–329.

[9]Juang, J.-N., and Pappa, R. S., "An Eigensystem Realization Algorithm for Modal Parameter Identification and Model Reduction," *Journal of Guidance, Control, and Dynamics*, Vol. 8, No. 5, 1985, pp. 620–627.

[10]Gregory, C. Z., Jr., "Reduction of Large Flexible Spacecraft Models Using Internal Balancing Theory," *Journal of Guidance, Control, and Dynamics*, Vol. 7, 1984, pp. 725–732.

[11]Boyd, S. P., and Barratt, C. H., *Linear Controller Design: Limits of Performance*, Prentice–Hall, Englewood Cliffs, NJ, 1991, Chap. 2.

[12]Lim, K. B., "Method for Optimal Actuator and Sensor Placement for Large Flexible Structures," *Journal of Guidance, Control, and Dynamics*, Vol. 15, No. 1, 1992, pp. 49–57.

[13]Doyle, J. C., Glover, K., Khargonekar, P., and Francis, B., "State-Space Solutions to Standard H_2 and H_∞ Control Problems," *IEEE Transactions on Automatic Control*, Vol. 34, No. 8, 1989, pp. 831–847.